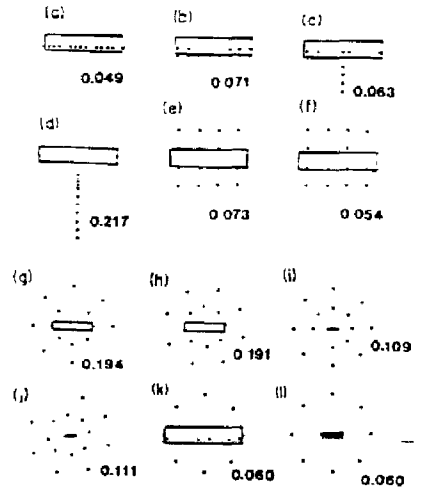

Fig. 3 Array configurations (plan views) tested for investigation of the optimum configuration for a dip-slip fault. The rectangle shows the fault and dots indicate stations. The numerical value indicates the accuracy of the inversion solution, σ.

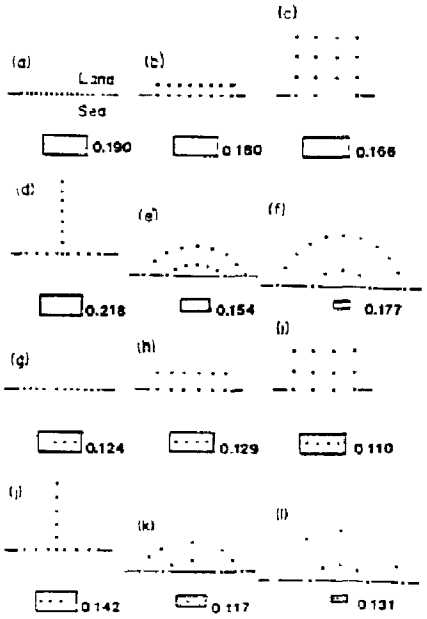

Fig. 4 Array configurations (plan views) tested for investigation of the optimum configuration for a subduction thrust fault. The thin horizontal line, the rectangle and the dots show, respectively, the coastline, the fault and stations. The numerical value indicates the accuracy of the inversion solution, σ.

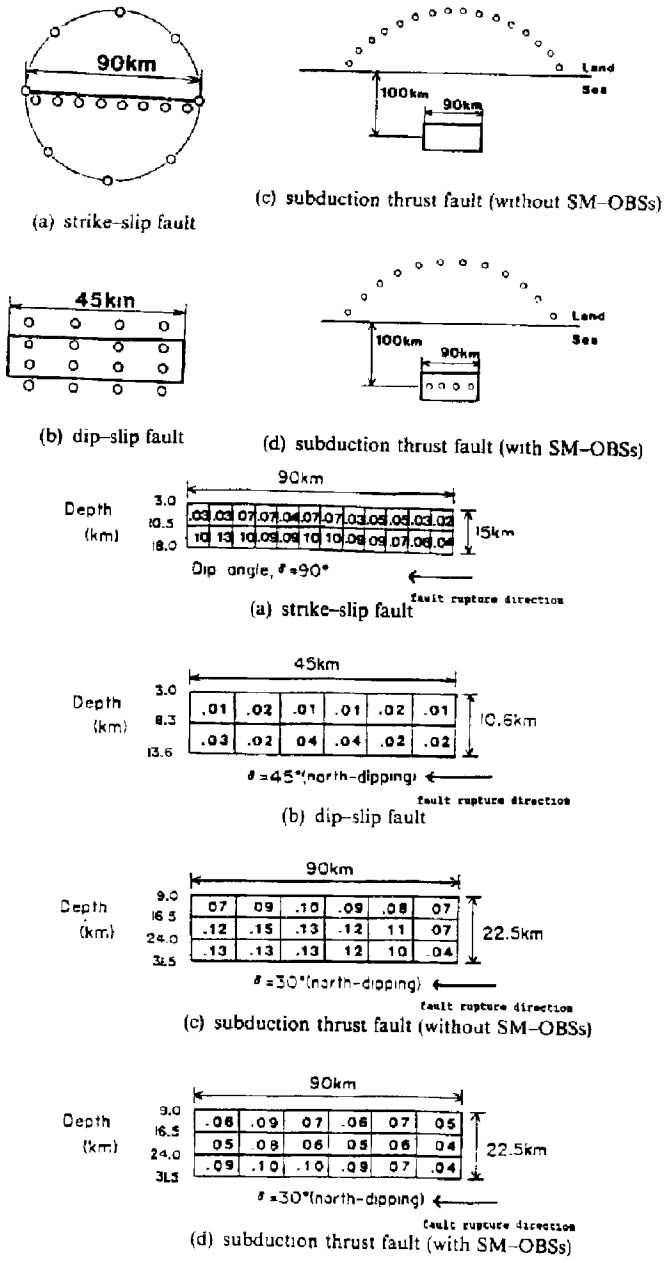

Fig. 5 The preferred array configuration and the distribution of the standard deviations of errors in estimating the seismic moment over the fault surface, which are obtained for each of three types of fault geometries: (a) strike-slip; (b) dip-slip; (c) (d) subduction thrust fault (two cases (c) with and (d) without strong-motion ocean bottom seismographs for the thrust fault).

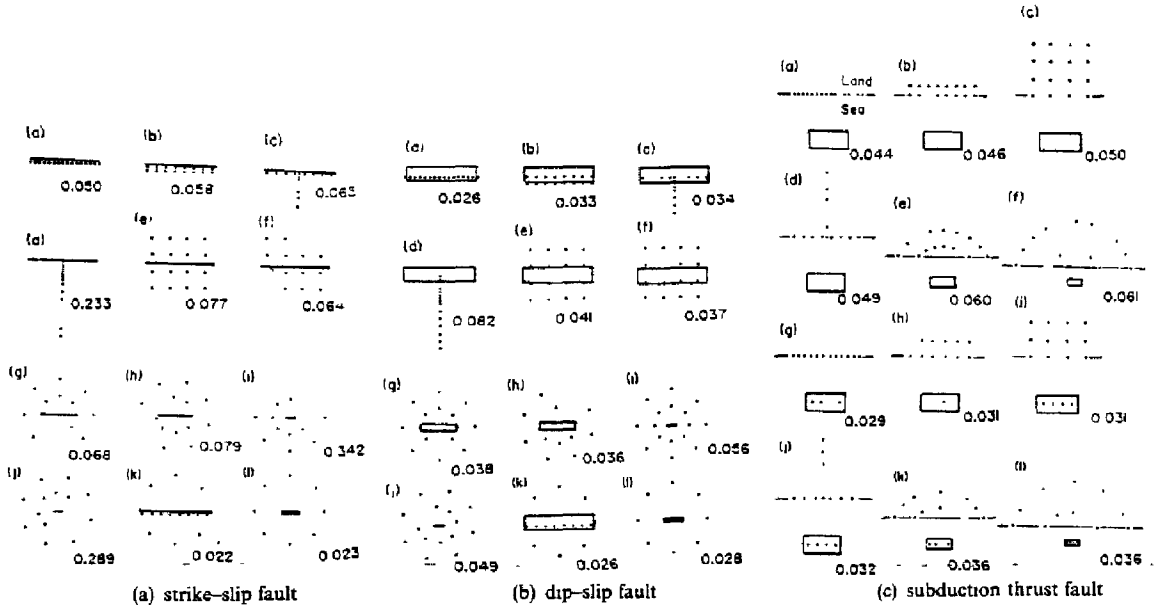

Fig. 6 The accuracies of the inversion solutions, σ, for various array configurations, which were obtained using only the far-field S waves for each of the same three types of fault geometries as in the present study: (a) strike-slip; (b) dip-slip, (c) subduction thrust fault.

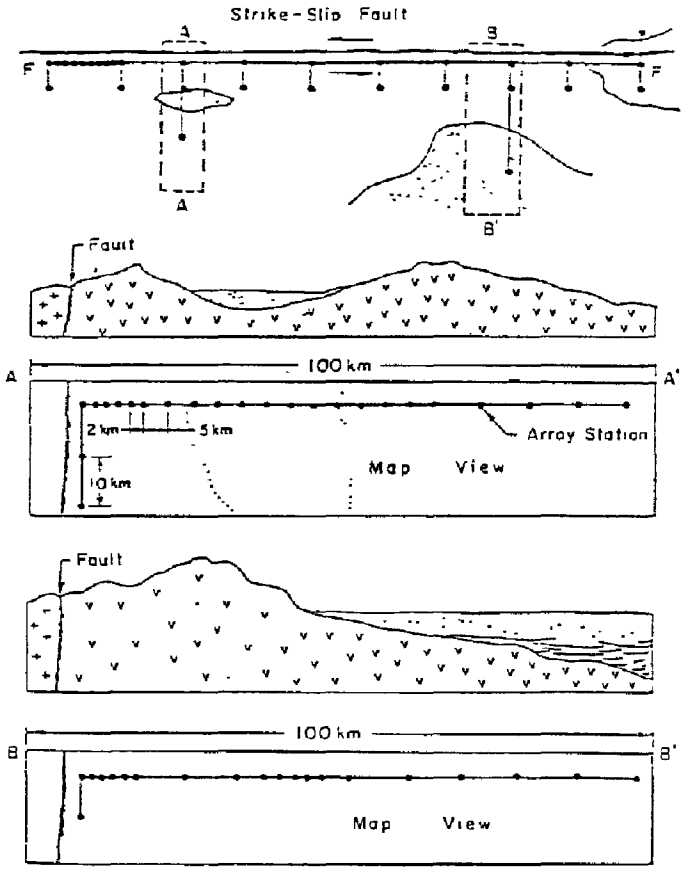

Fig. 7(a) Strike-slip fault

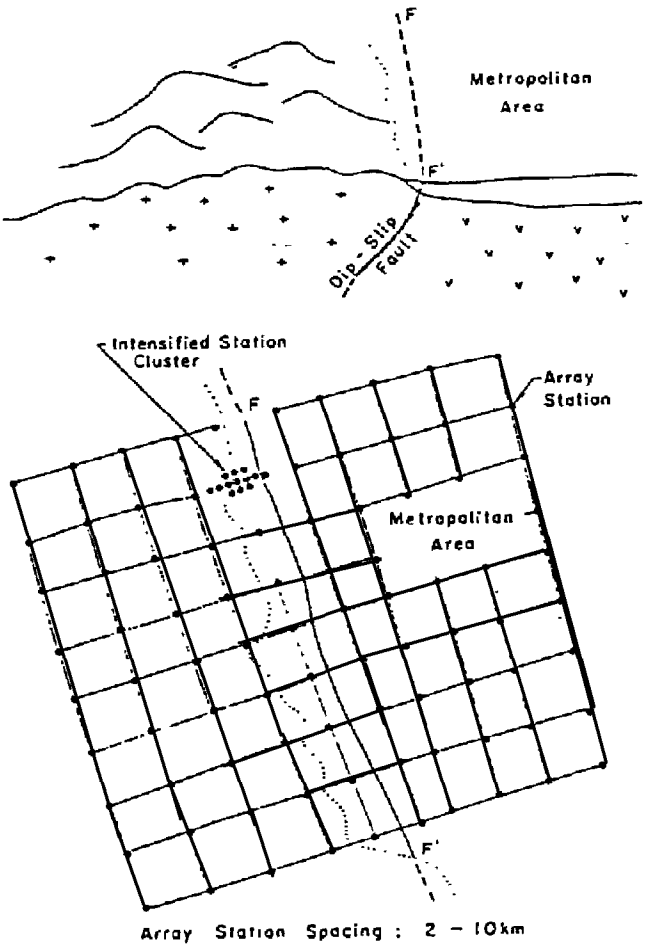

Fig. 7(b) Dip-slip fault

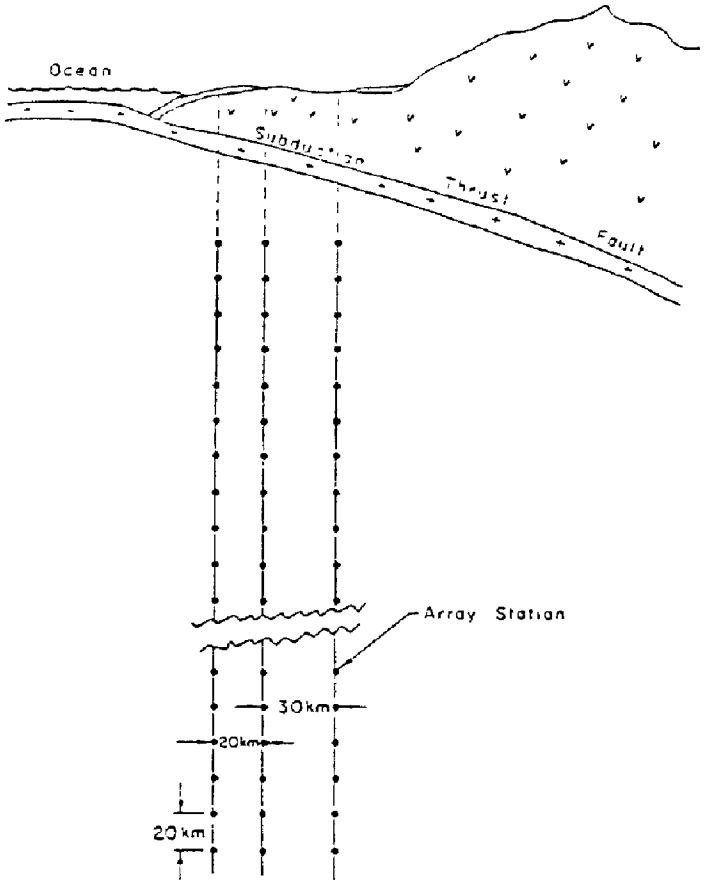

(c) Subduction thrust fault

Fig. 7 Array configurations for source mechanism and wave propagation studies recommended at the 1978 International Workshop on Strong-Motion Earthquake Instrument Arrays: (a) strike-slip; (b) dip-slip; (c) subduction thrust fault.

Lecture 2 ARRAY LAYOUT FOR SOURCE INVERSION

Subject 3 Preliminary Analysis of Resolving Power of Existing Strong-Motion Arrays for Source Inversion

1. INTRODUCTION

From the viewpoint of source inversion, we investigate the resolving power of four existing strong-motion arrays in this study: arrays for the 1979 Imperial Valley and the anticipated Parkfield, California earthquakes, and the 1968 Tokachi-Oki and the anticipated Tokai, Japan earthquakes. Our major goal is to provide guidelines for future planning installation of strong-motion array. We feel that the limitations of inversion studies imposed by the existing array should be first examined, following which reasonable guidelines for future installation will be deduced. We apply a method previously developed (Miyatake *et al.*, 1986, Iida *et al.*, 1990) to rupture models of the previous earthquakes and also to rupture models of the anticipated earthquakes. The accuracy of source inversion will be estimated for different number of stations in each array and for different target resolution. In the case of the Parkfield array, we try to suggest how the array could be improved by relocating four stations, although detailed discussion on each array are beyond the scope of this study. We calculate simplified theoretical seismograms by using Green's function for a half space (Kawasaki *et al.*, 1973); more realistic analysis of an array in the Los Angeles basin for source studies on the Whittier Narrows earthquake of 1987 will be given elsewhere (Iida *et al.*, in preparation).

This paper represents the fourth in a series of papers dealing with strong-motion array configuration for source studies. First, we developed a scheme to estimate the accuracy of the inversion solution on the basis of Wolberg's (1967) prediction analysis (Miyatake *et al.*, 1986). Second, we obtained relationships between the inversion accuracy and fault-array parameters (Iida *et al.*, 1990). Third, we proposed an optimum array geometry for a few typical types of earthquake faults (Iida *et al.*, 1988; Iida, 1990). As a natural extension of these studies, we apply the method to practical cases. Although numerous studies have been performed by using strong-motion datasets to infer rupturing processes of recent large earthquakes such as the 1979 Imperial Valley earthquake, the results do not necessarily agree with each other and the differences are not negligible.

Among the four cases to be studied, two are for strike-slip earthquakes, i.e., the Imperial Valley and the Parkfield arrays and the other two are for thrust events with relatively large strike-slip component, i.e., the Tokachi-Oki and the Tokai arrays. We investigate the Parkfield array installed by the end of 1985.

2. METHODS

In this study, the resolving power of the whole array is evaluated by utilizing theoretical array seismograms and a preliminary attempt is made to estimate the contribution of individual array stations. In this section the method of evaluating the whole array on the basis of expected accuracy of the inversion solution will be first described, and then a preliminary method of estimating station contributions will be introduced.

Since the method of evaluating an array for source studies has been explained in detail in previous studies (Miyatake *et al.*, 1986; Iida *et al.*, 1990), we will give here only a brief summary. In this method, the accuracy of source inversion is evaluated for a pair of target fault and specific strong-motion array by using the Wolberg's (1967) prediction analysis; we estimate the accuracy of the solution from errors in the data by using the principle of error propagations. This is done by solving normal equations for an overdetermined least-squares problem only once. A major advantage of this method is that repeated calculations in an actual inversion procedure is

---

* This lecture note is based on the paper of the same title written by Masahiro Iida, Takashi Miyatake and Kunihiko Shimazaki, published on "J. Phys. Earth, 38, 285-304, 1990".

unnecessary.

We treat a detailed rupturing behavior of an earthquake fault, so that we divide the entire fault into many subfaults and use the displacement waveform representation for a point source on each subfault to calculate synthetic seismograms. A common source time function appropriate for the subfault size is assumed for each subfault. We use the exact solutions (Kawasaki *et al.*, 1973) in a semi-infinite homogeneous space. A detailed study on a specific array which takes a regional layered structure into account is beyond the scope of this study, and will be given elsewhere (Iida *et al.*, in preparation).

The unknown parameters are the seismic moment and the rupture onset time for each subfault, which are determined so as to minimize the weighted sum of the squares of the residuals (O-C) of waveform at array stations. For evaluating the resolving power of the whole array, we use the maximum standard deviation of errors in estimating the seismic moment for each subfault. Errors in estimating the rupture onset time are found to be underestimated in our linear scheme and will not be used for the array evaluation (Miyatake *et al.*, 1986). In the following we use the maximum standard deviation, σ, of estimated subfault moment which is normalized by the given seismic moment.

Normally distributed errors are assumed for independent variables, the dip angle, the strike direction, and the slip angle of each subfault, and for the wave amplitude and the arrival time. The assumed standard deviations of the errors are given in Table 1. Here, errors in the dip angle and the strike direction also have a strong effect on the resolving power of the whole array The standard deviation of errors in measuring the wave amplitude is estimated from the level of ground noises and not from the instrumental capability. The required accuracy would be too high for certain types of accelerograph with relatively narrow dynamic range.

Table 1 Standard deviations of errors assumed in estimating the seismic moment and the rupture onset time for each subfault.

Dip angle	10.0°
Strike direction	10.0°
Slip angle	10.0°
Wave amplitude	0.01 cm
Arrival time	0.1 s

At this point it would be worthwhile to point out a major difference between our approach and ordinary scheme of source inversion. In our analysis, no constraint is added to stabilize solutions. Instead we require 'perfect' resolution, i.e., the resolution matrix is an identity matrix. In ordinary source inversion, the fault is divided into such a large number of small subfaults that the solution becomes unstable. The instability occurs due to an ill-conditioned matrix even in an overdetermined system of equations (e.g., Hartzell and Heaton, 1983). The resolution is sacrificed because of added constraints to stabilize the solution. In general, it is necessary to compromise two quantities, 'resolution' and 'variance' of the solution. In our analysis, we use 'variance' to estimate the uncertainty of the solution while we require perfect 'resolution'. Thus the subfault size is important in our analysis because it gives the resolution. On the other hand, it is rather insignificant in ordinary source inversion, because the effective resolving size is larger than the subfault area.

In an attempt to evaluate the contribution of each station, we rather intuitively introduce two key parameters: 'time separation' and 'moment sensitivity'. The time separation Δt at a specific station is defined by the minimum difference of arrival times between all kinds of seismic phases radiated from all subfaults. When the seismic phases are well separated in time, we can expect a good resolution of the solution. The moment sensitivity indicates how sensitive is the seismogram at a specific station to the moment of subfaults. It is defined by Σ_{ij} $(\sigma \Delta r_i / \sigma m_j)$, the summation over time and subfaults of the partial derivatives, where $\Delta r_i = |f(t_i)-s(t_i)|$ is the absolute residual of wave amplitude at the i-th time point ($f(t_i)$: observed and $s(t_i)$: synthetic seismograms), and m_j

is the seismic moment of the j-th subfault.

Our previous study (Iida *et al.*, 1988) shows that these two parameters are often complementary to each other. The most preferable array for source studies involves two different kinds of stations: stations aligned along a line parallel and close to the fault, and stations surrounding the fault with good azimuthal coverage. There is some tendency that the former type of array station usually has a relatively large value of 'moment sensitivity' while the latter type of array station generally has a large value of 'time separation'.

Figure 1 (Iida *et al.*, 1988) shows an example; it compares three different types of array configuration for a unilateral rupture of a shallow strike-slip fault. The numerical value at each subfault indicates the standard deviation of errors in estimating the seismic moment, normalized by the seismic moment, for each subfault. Its maximum is shown below the schematic array configuration. Note that the maximum normalized standard deviation is used for evaluating arrays throughout this study.

Figure 1 suggests that stations aligned along a line parallel and close to the fault help to resolve the later part of the fault rupturing process while stations surrounding the fault with good azimuthal coverage help to resolve the earlier part When only the stations close to the fault and aligned parallel to its strike are used (Fig. 1a), the seismic moment in the earlier stage of rupturing cannot be inferred with high accuracy. On the other hand, when only the stations surrounding the fault are used (Fig. 1b), the seismic moment in the later stage of rupturing cannot be inferred with high accuracy. The combined one of a line-segment array and a circular array is the most preferable (Fig. 1c).

Figure 2 shows the value of the two key parameters at each station for the three types of array configuration corresponding to the cases in Fig. 1. In this figure, instead of $\Sigma_{i,j}$ $(\sigma\Delta r_i/\sigma m_j)$, $\Sigma_{i,j}$ $(\sigma\Delta r_i/\sigma D_j)$ is used for simplicity, where D_j is the amount of dislocation on the j-th subfault. The residual Δr_i is defined as the average of the three axial components.

All the stations in the line-segment array in Fig. 1a show a large value of the moment sensitivity (Fig. 2a) while most of the stations in the circular array in Fig. 1b take a small value (Fig. 2b). On the other hand, the time separation is generally large at stations of the circular array, but it is small at stations of the line-segment array except for stations from which the rupture propagates away. In the most preferable array (Fig. 1c), stations with large moment sensitivity and stations with large time separation are complementarily combined (Fig. 2c).

As was shown above, the two key parameters show the contribution of each station to some extent. However, note that they do not represent any combined effect of stations, but show certain features of single station. In particular, the time separation parameter is occasionally subject to a small change in station location with extreme subtlety. For example, at station numbered 5 in Fig. 1b, it takes an extremely small value compared with the neighboring stations

3. FAULTS AND ARRAYS EXAMINED

Assumed values of fault parameters for the four earthquakes studied here are summarized in Table 2 These values are mainly quoted from Hartzell and Helmberger (1982) and Olson and Apsel (1982) for the 1979 Imperial Valley earthquake, from Spudich and Oppenheimer (1986) for the anticipated Parkfield earthquake, from Kanamori (1971) for the 1968 Tokachi-Oki earthquake, and from Ishibashi (1981) for the anticipated Tokai earthquake. Two fault models with different subfault sizes are tested for respective earthquakes Three rupturing modes are assumed only for the anticipated Tokai earthquake. The sampling time intervals used for the 1979 Imperial Valley, the anticipated Parkfield, the 1968 Tokachi-Oki, and the anticipated Tokai earthquakes are, respectively, 0.5, 0.4, 1.0 and 1.2 s. The main features of the arrays and the faults will be given in the following.

Table 2. Fault parameters assumed for estimating the effectiveness of the four existing strong-motion array networks.

Earthquake	1979 Imperial Valley	Anticipated Parkfield	1968 Tokachi-Oki	Anticipated Tokai
Fault area	50 km × 10 km 48 km × 9 km	30 km × 10 km 30 km × 12 km	150 km × 90 km 160 km × 100 km	125 km × 75 km 120 km × 75 km
Number of fault elements	20 (= 10 × 2) 48 (= 16 × 3)	12 (= 6 × 2) 40 (= 10 × 4)	15 (= 5 × 3) 40 (= 8 × 5)	15 (= 5 × 3) 40 (= 8 × 5)
Subfault area	5 km × 5 km 3 km × 3 km	5 km × 5 km 3 km × 3 km	30 km × 30 km 20 km × 20 km	25 km × 25 km 15 km × 15 km
Strike (clockwise from N)	143.0°	139.0°	156.0°	18.0°
Dip angle	90.0°	90.0°	20.0°	34.0°
Slip direction	0.0°	0.0°	38.0°	71.0°
Final offset	1.0 m	0.6 m	4.1 m	4.0 m
Rupture mode	Bilateral	Bilateral	Unilateral	Unilateral (two cases) and bilateral
Rupture velocity	2.5 km/s	2.5 km/s	3.5 km/s	2.5 km/s
Depth of fault top	2 km	1 km	17.6 km 15.9 km	2 km
S-wave velocity	3.0 km/s	3.5 km/s	4.0 km/s	3.5 km/s
Medium density	3.0 g/cm^3	3.0 g/cm^3	3.0 g/cm^3	3.0 g/cm^3
Quality factor	300.0	300.0	500.0	300.0

(A) The 1979 Imperial Valley earthquake

Strong-motion recordings of the 1979 Imperial Valley earthquake, the best-instrumented moderate-size event to date, provided us with a unique opportunity to construct a realistic model of rupture history and wave propagation for this earthquake. Not a few studies (e.g., Hartzell and Helmberger, 1982; Olson and Apsel, 1982; Hartzell and Heaton, 1983; Archuleta, 1984; Silver and Masuda, 1985) estimated the distribution of slip for this earthquake using the strong-motion data set. The determined fault model is right-lateral vertical strike slip with a dislocation of roughly 1 m as an average. The surface fault trace of this earthquake and the locations of strong-motion recording stations are shown in Fig. 3a. The El Centro strong-motion array perpendicularly crossing the fault trace is composed of 13 stations, which are indicated by the solid squares. Only a few stations are installed at the immediate vicinity of the fault, and also the azimuthal coverage of the fault is relatively poor.

(B) The anticipated Parkfield earthquake

Moderate-size earthquakes occurred at remarkably regular intervals in the Parkfield section of the San Andreas fault. The next characteristic Parkfield earthquake is expected to occur within a four-year period centered on 1987-1988 according to a simple recurrence model that explains most of the historic seismicity (Bakun and Lindh, 1985).

For the purpose of measuring ground shaking close to the earthquake fault, a strong-motion array was recently deployed by the California Strong-Motion Instrumentation Program (CSMIP) in the vicinity of Parkfield (McJunkin and Shakal, 1983). The configuration of the Parkfield strong-motion array was designed fairly completely in order to provide primarily near-fault ground motion data by which details of the fault rupturing process may be resolved. As shown in Fig. 4a, the array comprises central near-fault stations paralleling the fault strike, complimented by three lines of stations extending perpendicularly to the fault strike. In total, 46 strong-motion stations were installed by the end of 1985. Roughly speaking, the array configuration is apparently satisfactory except for the sparsity of stations on the northwestern side of the fault. Because the last three Parkfield events which occurred on the San Andreas fault had a similar characteristic, the values of fault parameters for the hypothetical earthquake can be easily estimated (Spudich and Oppenheimer, 1986).

(C) The 1968 Tokachi-Oki earthquake

Various studies on the 1968 Tokachi-Oki earthquake (e.g. Kanamori, 1971; Fukao and Furumoto, 1975; Iida and Hakuno, 1984; Mori and Shimazaki, 1984, 1985; Kikuchi and Fukao, 1985) revealed the complicated fault

rupturing process of this earthquake which consists of a few stages This earthquake provided instructive information on the fault rupturing mode because it was one of a few great earthquakes that recently occurred in Japan. No specific strong-motion array existed at the occurrence time of this earthquake, but owing to the fault location at the arc-arc junction, a number of strong-motion stations encircled the fault area with a relatively good azimuthal coverage as shown in Fig. 5. The effectiveness of strong-motion ocean bottom stations installed within the fault area will be also examined

(D) The anticipated Tokai earthquake

At the 1978 International Workshop on Strong-Motion Earthquake Instrument Arrays (Iwan, 1978), the Suruga-Izu, Japan, area was designated as one of the six high-priority areas that were considered as being promising for the deployment of strong-motion arrays. According to Ishibashi (1981), both the seismic gap and the considerable amount of strain accumulation estimated from geodetic survey suggest a fairly high probability of a large earthquake occurrence in the near future. He concluded that the most probable rupture area of the next large interplate earthquake would be mainly the Suruga-trough thrust beneath Suruga Bay He also proposed a static fault model for the future Tokai earthquake as the first-order approximation on the assumption that the fault area is equivalent to the northeastern part of the 1854 Ansei Tokai earthquake fault.

Following a recommendation at the International Workshop, a strong-motion array composed of 18 digital accelerographs with a 20-30 km station spacing was deployed in this region (Tanaka *et al* , 1984) (Fig. 6a). Besides this array, several stations are distributed in this area (stations numbered 19-24 and 29-33 in Fig. 6b). The anticipated Tokai earthquake is of major interest because approximately one half of the predicted fault area underthrusts beneath the land.

4. RESULTS

The results which have been derived from the simulations are summarized in Table 3, and are illustrated in Figs. 3 through 6. The resolving power of the whole array indicated in Table 3 shows the maximum standard deviation of errors in estimating the subfault seismic moments, which is normalized by the seismic moment. As a rough estimate, for example, 0.08 is considered as an 8% error. These values are used as an objective indicator for estimating the reliability of inversion calculations. First of all, we find that the subfault size is the dominant factor in all cases. In Figs. 3 through 6, the uncertainty of the inversion solution at all the subfaults is indicated by ranking. The inversion uncertainty means the standard deviation of errors in estimating the subfault seismic moment, normalized by the seismic moment itself.

We also show 'time separation' and 'moment sensitivity' at individual array stations. These are considered as indicators of the contribution of individual stations. Actually, instead of $\Sigma_{i,j}$ $(\sigma\Delta r_i/\sigma m_j)$, $\Sigma_{i,j}$ $(\sigma\Delta r_i/\sigma D_j)$ is used for simplicity, where D_j is the amount of dislocation on the j-th subfault. The time separation is shown by the length of the vertical bar and the moment sensitivity by the length of the horizontal bar.

(A) The 1979 Imperial Valley earthquake

Three cases of station arrays are tested for the 1979 Imperial Valley earthquake as in Miyatake *et al.* (1986). They are 1) the El Centro array perpendicularly crossing the fault trace (13 stations, indicated by the solid squares in Fig 3), 2) 20 stations distributed within the United States (the solid and open squares), and 3) all the 26 stations shown in the figure

If the fault is divided into subfaults as small as 3 km x 3 km, the error becomes unacceptably large. We also find rather drastic change in the inversion uncertainty at each subfault due to the change in the number of stations used (Fig. 3c).

Table 3. The resolving power of the whole array can be estimated by the maximum standard deviation of errors in estimating subfault seismic moments, normalized by the seismic moment.

(A) The 1979 Imperial Valley earthquake

N_f	N_s		
	13	20	26
20 (5 × 5 km²)	0 88	0.41	0.18
48 (3 × 3 km²)	5 46	3 19	0.94

(B) The anticipated Parkfield earthquake

N_f	N_s		
	14	22	46
12 (5 × 5 km²)	0.49	0.22	0.14
40 (3 × 3 km²)	4 43	2 43	1 83

(C) The 1968 Tokachi-Oki earthquake

N_f	N_s		
	8	12	16
15 (30 × 30 km²)	0.23	0 17	0.09
40 (20 × 20 km²)	1.35	0.83	0.41

(D) The anticipated Tokai earthquake

N_f	Rupture mode*	N_s				
		8	18	13	25	29
15 (25 × 25 km²)	1	0.52	0.23	0.34	0.15	0 12
	2	0 54	0 27	0 32	0 14	0 12
	3	0.37	0.21	0.19	0.08	0 07
40 (15 × 15 km²)	1	2.79	1 10	1.86	0 64	0 62
	2	2.94	1 10	1.96	0 72	0.68
	3	2.30	1.60	1.01	0 47	0 46

The number of fault elements and the number of stations are denoted by N_f and N_s, respectively. The numerical value inside the parenthesis shows the subfault area.

* (1) Unilateral rupture starting from the northern end, (2) Bilateral rupture starting from the center of the fault, (3) Unilateral rupture starting from the southern end

There exists a large variation in the inversion uncertainty among the subfaults, and the largest error occurs at the subfault on the southeastern end, when the Mexican stations are not used. It indicates an important contribution of the Mexican stations to the improvement of the array, which is probably due to a better azimuthal coverage. The large uncertainty for a case of the El Centro array is a clear indication that a linear array of stations perpendicularly crossing the fault is impertinent to source inversion as was shown by Miyatake *et al.* (1986). The strong dependency of the resolving power on the array configuration for a vertical strike-slip fault (Iida *et al.*, 1988) requires a careful installation of array stations for this type of fault. On the basis of the two key parameters, the most effective stations appear to be located closely to the fault trace or on its southeastern extension (Fig. 3a and b).

(B) The anticipated Parkfield earthquake

Three array configurations tested for the anticipated Parkfield earthquake are shown in Fig. 4a. They are 1) 14 stations aligned along the fault trace (the solid squares in the figure), 2) 8 stations aligned perpendicular to the fault trace added to the 14 stations (in total, 22 stations, the solid and open squares), and 3) all the 46 stations.

A 3 km x 3 km subfault is the minimum size allowable to perform a meaningful source inversion. The Parkfield array is apparently satisfactory because the inversion uncertainty of individual subfaults shows a small

variation on the fault (Fig. 4b). A rather poor station coverage on the northwestern side appears to cause the largest error at the subfault on the northwestern end. We will show in the next section that this array can be largely improved by relocating only four stations. On the basis of the results on the Imperial Valley array, four limbs oriented perpendicular to the fault trace do not seem to be effective for source inversion studies. In addition, the two key parameters suggest that effective stations are concentrated along the fault trace (Fig. 4a).

(C) The 1968 Tokachi-Oki earthquake

Three arrays examined for the 1968 Tokachi-Oki earthquake are shown in Fig. 5. They are shown 1) by the solid squares in the figure (8 land stations), and 2) by the solid and open squares (12 land stations including one hypothetical station numbered 10), and 3) by all the symbols (16 stations in total, including 4 hypothetical ocean bottom stations installed within the fault area, indicated by the solid circles).

So far as only land stations are used, a reliable inversion cannot be expected for subfaults as small as 20 km x 20 km. The largest error takes place just south of the center of fault with σ amounting to 1.35 and 0.83 for the cases of 8 and 12 land stations, respectively. Also the inversion uncertainty varies considerably from subfault to subfault.

Although distant stations are relatively useful for this type of shallowly dipping dip-slip fault (Iida *et al.*, 1990), the installation of ocean bottom stations within the fault area averages the inversion uncertainty over the fault area (Fig. 5), resulting in a decrease of the largest error. The maximum normalized uncertainty σ decreases to 0.41 for 20 km x 20 km subfaults and it becomes as small as 0.09 when we choose subfault size of 30 km x 30 km.

Whereas large values of the moment sensitivity are restricted to the ocean bottom stations within the fault area, the stations with large time separation appear to lie on the northern and southwestern sides of the fault (Fig. 5).

(D) The anticipated Tokai earthquake

Five array examined for the anticipated Tokai earthquake are shown in Fig. 6a and b. In Fig. 6a, they are shown 1) by the solid squares (8 stations involved in the Suruga-Izu array), and 2) by the solid squares and the solid triangles (all 18 stations of the Suruga-Izu array). In Fig. 6b, they are shown 3) by the open and solid squares (13 land stations), and 4) by all the squares and the open triangles (25 land stations including 4 hypothetical stations numbered 25 to 28), and 5) by all the symbols (29 stations including 4 hypothetical ocean bottom stations indicated by the solid circles).

The resolving power is greatly dependent on the direction of rupture propagation. Also the time separation at each station varies with the rupturing direction (Fig. 6a and b). Figure 6c compares the distributions of inversion uncertainty on the fault for three different modes of rupture propagation. These correspond to a case for 15 km x 15 km subfaults and 29 stations. The maximum uncertainty becomes relatively small when the rupture unilaterally propagates northward. In other words, the southern part of the fault becomes relatively well resolved if it ruptures in the earlier part of the entire rupturing process. Referring to the results shown in Fig. 1, this is probably due to the relatively good azimuthal coverage owing to many land stations surrounding the fault. Several land stations located within the northern part of the fault help to resolve the later part of the rupturing process. On the other hand, if the southern part of the fault ruptures in the later stage of rupturing process, the inversion uncertainty becomes large because of poor station coverage of the southern oceanic part of the fault

By using the land network alone, a reliable inversion solution will be obtained only for subfaults larger than 15 km x 15 km. We recommend an addition of more stations in the west and north of the fault on the basis of the results shown in Table 3. In the case of subfault size of 25 km x 25 km, the hypothetical array of 25 land stations gives σ = 0.08-0.15 while the present Izu-Suruga array gives σ = 0.21-0.27.

When the number of stations increase, the variation in inversion uncertainty among the subfaults generally decreases, resulting in a decrease of the largest uncertainty. However, we do not recommend an installation of ocean bottom stations in the fault area, because their effect is found to be unexpectedly small.

5. DISCUSSION

The method described above can be applied to the improvement of existing arrays. In this section, this is attempted for the Parkfield array (Fig. 7a). In the first simulation, we examine how the array can be improved by relocating only four stations. In the second simulation, we attempt to acquire the same resolving power as the original Parkfield array of 46 stations with a better distribution of fewer stations.

Figure 4b shows that the inversion uncertainty is the largest on a subfault at the northwestern end of the fault. The distribution of uncertainty on the fault looks somewhat similar to that shown in case (2) of Fig. 3c, which corresponds to the array of all 20 U.S. stations for the Imperial Valley earthquake. In this case for the Imperial Valley event, the largest uncertainty takes place on a subfault on the southeastern end because the Mexican stations are not used. This suggests that the inversion uncertainty for the Parkfield event would decrease if we install stations in the northwestern part of the fault.

In the first simulation, we test three cases. We remove four southern stations numbered 38, 40, 42 and 44 in Fig. 7a, and add four new ones in three different manners. Then we estimate the resolving power of each new array. The four removed stations are chosen because both the time separation and the moment sensitivity at these stations are small compared with the neighboring stations and also because they are in an area of the most dense installation. The three kinds of arrays tested are shown in Fig. 7b, c and d together with the largest uncertainty estimated. We should note that the resolving power of the whole array is surprisingly improved by adding stations in the northwestern part of the fault as was expected (Fig 7b). Adding stations in distant areas for a better azimuthal coverage of the northwestern end of the fault also improves the resolving power (Fig. 7d). Figure 7c shows that the linear array oriented perpendicular to the fault trace only slightly improves the resolving power.

The results that have been derived from another simulation are shown in Fig. 8. This simulation is aimed at showing a desirable array configuration for the target fault. With 30 stations distributed in Fig. 8c, a slighily better resolving power is acquired (the largest uncertainty is 0.130) than that for the original array (0.138). A comparatively good resolving power can be expected for arrays of even fewer stations. These results will guide us how to arrange array stations. We can conclude that the larger number of stations which surround the fault with satisfactory azimuthal coverage would help to enhance the resolving power of the whole array.

In the actual Parkfield array, more stations have been installed since the end of 1985. Thus the points discussed above on the Parkfield array installed by the end of 1985 have been already improved. U.S. Geological Survey installed 7 force-balance accelerometers in the northwestern side of the fault as a part of the General Earthquake Observation System (Bakun, 1988).

The method described in this study can offer a guideline for future planning installations of strong-motion arrays and for reasonable addition, removal and relocation of stations of existing arrays. Although the two key parameters, 'time separation' and 'moment sensitivity', are not complete in explaining the effectiveness of various array stations, it is highly probable that array stations which have small values of the two parameters are ineffective.

Also, it has been demonstrated in this study that the deployment of strong-motion, ocean bottom seismographs should be taken into account in future planning installations for offshore faults such as the 1968 Tokachi-Oki earthquake fault. Today, semi-permanent SM-OBSs are not in operation, but temporary networks of SM-OBS systems are in the process of development since 1978. The experiments indicate that ocean bottom stations are capable of recording ground accelerations up to about 1.0 g in the 0.1 to 10 Hz frequency band with good reliability in most cohesive-type soil conditions (Steinmetz *et al.*, 1979; Steinmetz *et al.*, 1981).

Finally, we should add that a differential array is another useful type available for source inversion studies. Since a difference in the arrival times of distinguishable phases is used for this analysis, our method cannot be applied directly to a differential array. Differential arrays were or are being installed for the 1979 Imperial Valley

earthquake fault (Spudich and Cranswick, 1984), for the anticipated Parkfield earthquake fault (Spudich and Oppenheimer, 1986), and for the anticipated Tokai earthquake fault (Okubo *et al.*, 1982).

6. CONCLUSIONS

The effectiveness of existing strong-motion arrays for source inversion studies has been investigated by estimating the accuracy of the inversion solution using the array seismograms. The resolving power of the whole array has been examined for different subfault sizes and for different configuration of array stations and the contribution of individual stations has been suggested for the four existing array networks. They are for the 1979 Imperial Valley, the anticipated Parkfield, the 1968 Tokachi-Oki, and the anticipated Tokai earthquakes.

The main results are summarized in the following:

1) The station array used for an analysis of the 1979 Imperial Valley earthquake is not suitable for source studies; especially the El Centro array, a linear array crossing perpendicularly the fault trace, is ineffective.

2) The station array installed by the end of 1985 for the anticipated Parkfield earthquake seems to be satisfactory because of the intensive installation of many stations. However, adding a few stations in the northwestern part of the fault or in distant areas for a better azimuthal coverage in the northwest of the fault further increases the resolving power of the whole array.

3) Detailed source inversion analysis cannot be expected for the 1968 Tokachi-Oki earthquake because of both the large fault area and lack of offshore stations. Strong-motion, ocean bottom instruments within the fault area are required for a further improvement of the inversion analysis.

4) An addition of several stations on the west and north sides of the fault area is desirable to the present network for the anticipated Tokai earthquake. The resolving power of the whole array for this earthquake is strongly dependent on a rupturing direction because station coverage of the southern oceanic part of the fault tends to be poor

In conclusion, several near-fault stations and more stations encircling the fault with good azimuthal coverage are primarily required for a strong-motion array to investigate source effects

7. REFERENCES

Archuleta, R.J. (1984). A faulting model for the 1979 Imperial Valley earthquake, *J. Geophys. Res.*, **89**, 4559-4585.

Bakun, W H. (1988). Geophysical instrumentation near Parkfield, *Earthq. Volcs.*, **20**, 60-71.

Bakun, W.H. and A.G. Lindh (1985). The Parkfield, California, prediction experiment, *Earthq. Predict. Res.*, **3**, 285-304.

Fukao, Y. and M. Furumoto (1975). Foreshocks and multiple shocks of large earthquakes, *Phys. Earth. Planet. Inter.*, **10**, 355-368.

Hartzell, S.H. and T.H. Heaton (1983). Inversion of strong ground motion and teleseismic waveform data for the rupture history of the 1979 Imperial Valley, California, earthquake, *Bull. Seismol. Soc. Am.*, **73**, 1553-1583.

Hartzell, S. and D.V. Helmberger (1982). Strong-motion modeling of the Imperial Valley earthquake of

1979, *Bull. Seismol. Soc. Am.*, **72**, 571-596.

Iida, M. (1990). Optimum strong-motion array geometry for source inversion - II, *Earthq. Eng. Struct. Dyn.*, **19**, 35-44.

Iida, M. and M. Hakuno (1984). The difference in the complexities between the 1978 Miyagi-Oki earthquake and the 1968 Tokachi-Oki earthquake from a viewpoint of the short-period range, *Nat. Disast. Sci.*, **6**, 1-26.

Iida, M., T. Miyatake and K. Shimazaki (1988). Optimum strong-motion array geometry for source inversion, *Earthq. Eng. Struct. Dyn.*, **16**, 1213-1225.

Iida, M., T. Miyatake and K. Shimazaki (1990). Relationship between strong motion array parameters and the accuracy of source inversion, and physical waves, *Bull. Seismol. Soc. Am.*, **80**, 1533-1552.

Ishibashi, K. (1981). Specification of a soon-to-occur seismic faulting in the Tokai district, central Japan, based upon seismotectonics, in *Earthquake Prediction - An International Review, Maurice Ewing Series*, ed. D.W. Simpson and P.G. Richards, Vol. 4, pp. 297-332, Am. Geophys. Union, Washington. D.C.

Iwan, W.D. (ed.) (1978). Strong-motion earthquake instrument array, Proc. Internatl. Workshop on Strong-Motion Earthquake Instrument Arrays, Honolulu.

Kanamori, H. (1971). Focal mechanism of the Tokachi-Oki earthquake of May 16, 1968: contortion of the lithosphere at a junction of two trenches, *Tectonophysics*, **12**, 1-13.

Kawasaki, I., Y Suzuki and R. Sato (1973). Seismic waves due to a shear fault in a semi-infinite media. Part I. Point source, *J. Phys. Earth*, **21**, 251-284.

Kikuchi, M. and Y. Fukao (1985). Iterative deconvolution of complex body waves from great earthquakes - the Tokachi-Oki earthquake of 1968, *Phys. Earth Planet. Inter.*, **37**, 235-248.

McJunkin, R.D. and A.F. Shakal (1983). The Parkfield strong-motion array, *Calif. Geol.*, **36**, 27-34.

Miyatake, T., M. Iida and K. Shimazaki (1986). The effects of strong-motion array configuration on source inversion, *Bull. Seismol. Soc. Am.*, **76**, 1173-1185.

Mori, J. and K. Shimazaki (1984). High stress drops of short-period subevents from the 1968 Tokachi-Oki earthquake as observed on strong-motion records, *Bull. Seismol. Soc. Am.*, **74**, 1529-1544.

Mori, J. and K. Shimazaki (1985). Inversion of intermediate-period Rayleigh waves for source characteristics of the 1968 Tokachi-Oki earthquake, *J Geophys. Res.*, **90**, 11374-11382.

Okubo, T., T. Arakawa and K. Kawashima (1982). Dense instrument array observation by the Public Works Research Institute and analysis of some records, 6th Japan Earthquake Engineering Symposium, 297-304 (in Japanese).

Olson, A.H. and R Apsel (1982). Finite faults and inverse theory with applications to the 1979 Imperial Valley earthquake, *Bull. Seismol. Soc. Am.*, **72**, 1969-2001.

Silver, P. and T. Masuda (1985). A source extent analysis of the Imperial Valley earthquake of October 15, 1979, and the Victoria earthquake of June 9, 1980, *J. Geophys. Res.*, **90**, 7639-7652.

Spudich, P and E. Cranswick (1984). Direct observation of rupture propagation during the 1979 Imperial

Valley earthquake using a short baseline accelerometer array, *Bull. Seismol. Soc. Am.*, **74**, 2083-2114.

Spudich, P. and D Oppenheimer (1986). Dense seismograph array observations of earthquake rupture dynamics, in *Earthquake Source Mechanics, Geophys. Monograph*, ed. S. Das, **37**, 285-296.

Steinmetz, R.L , P.L. Donoho, J.D. Murff and G.V. Latham (1979). Soil coupling of a strong motion, ocean bottom seismometer, 11th Offshore Technology Conference Proceedings, **4**, 2235-2249.

Steinmetz, R L., J.D. Murff, G. Latham, A. Roberts, P. Donoho, L. Babb and T. Eichel (1981).. Seismic instrumentation of the Kodiak Shelf, Marine Geotechnology, **4**, 192-221.

Tanaka, T., K. Kudo, M. Sakaue, E. Shima and Y. Osawa (1984). An observation network of earthquake strong motion in the Sagami Bay region and the Izu Peninsula, 8th World Conference on Earthquake Engineering, **2**, 15-22.

Wolberg, J.R. (1967). *Prediction Analysis*, D. Van Nostrand Co. Inc., Princeton, New Jersey.

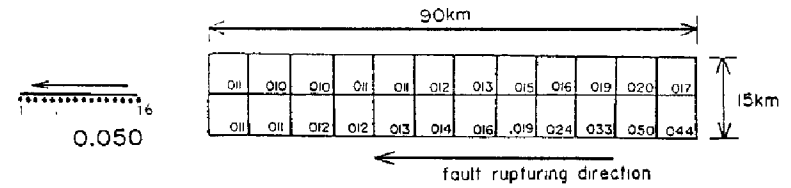

(a) Line-segment array parallel and close to the fault

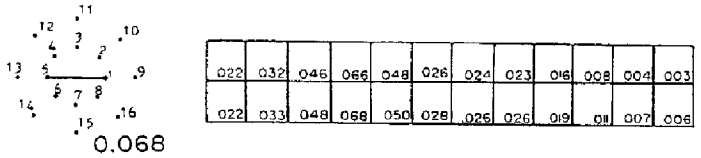

(b) Concentric circular array encircling the fault

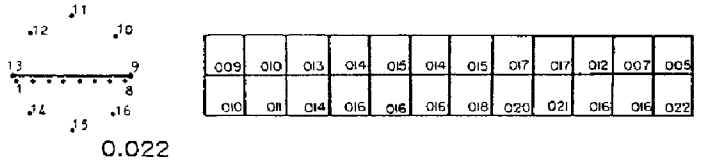

(c) Combined array of a line segment and a circle

Fig. 1 The uncertainty of inversion solution estimated at all the subfaults for unilateral rupture of a strike-slip fault (Iida *et al.*, 1988). Three different array configurations are illustrated. The inversion uncertainty means the standard deviation of errors in estimating the subfault seismic moment, normalized by the seismic moment itself. The value shown on the left together with the schematic array configuration indicates the maximum uncertainty obtained among all subfaults. Note small uncertainty on the left half of the fault (i.e., in the later part of the rupturing process) for the line-segment array (a), and on the right half of the fault (i.e., in the earlier part of the rupturing process) for the circular array (b). For the combined array (c), the uncertainty becomes small over the entire part of the fault. In this calculation only the far-field S waves are used for theoretical seismograms as was adopted in Miyatake *et al.* (1986) while the exact Green's function for homogeneous half space is used for other results shown in this study.

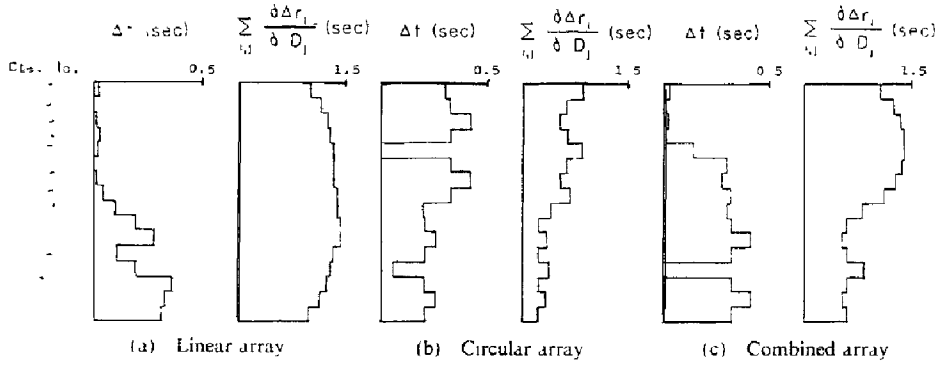

Fig. 2 The two key parameters calculated for stations in three different array configurations shown in Fig. 1. One of the parameters, 'time separation,' shows the minimum difference of arrival times between all the seismic waves radiated from subfaults. This parameter is generally large for an array with good azimuthal coverage (e.g., case (b)). The other parameter, 'moment sensitivity,' indicates how sensitive is the seismogram at a specific station to the moment of subfaults It is defined by $\Sigma_{i,j}(\sigma\Delta r_i/\sigma m_j)$, the summation over time and subfaults of the partial derivatives, where $\Delta r_i = |f(t_i)-s(t_i)|$ is the absolute residual of wave amplitude at the i-th time point ($f(t_i)$: observed and $s(t_i)$: synthetic seismograms), and m_j is the seismic moment of the j-th subfault. In the figure $\Sigma_{i,j}(\sigma\Delta r_i/\sigma D_j)$ is shown instead of $\Sigma_{i,j}(\sigma\Delta r_i/\sigma m_j)$, where D_j indicates the amount of dislocation on the j-th subfault. This parameter is generally large at near-source stations (e.g., case (a)).

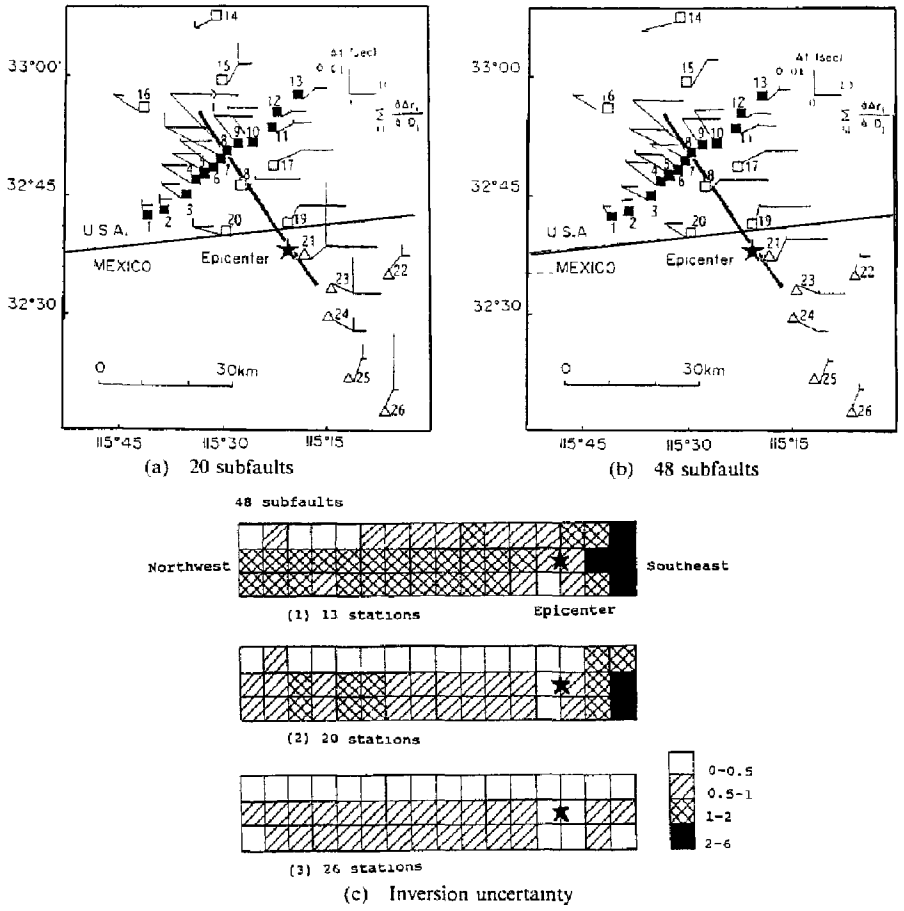

Fig. 3 Location map of the Imperial Valley section of the San Andreas fault showing the fault trace of the 1979 Imperial Valley earthquake and the strong-motion recording stations in (a) and (b), and the inversion uncertainty at all the subfaults in (c). Three station arrays examined are 1) El Centro array perpendicularly crossing the fault trace (13 stations, indicated by the solid squares), 2) 20 stations distributed within the United States (the solid and open squares), and 3) all the 26 stations. The inversion uncertainty at 48 subfaults determined for the three kinds of arrays (13, 20 and 26 stations) is indicated by ranking in (c). The inversion uncertainty means the standard deviation of errors in estimating the subfault seismic moment, normalized by the seismic moment itself. 'Time separation' and 'moment sensitivity' are also evaluated at individual stations for the cases of (a) 20 and (b) 48 subfaults. The length of vertical bars shows the time separation and that of horizontal bars shows the moment sensitivity. For 'time separation' and 'moment sensitivity,' see caption of Fig. 2.

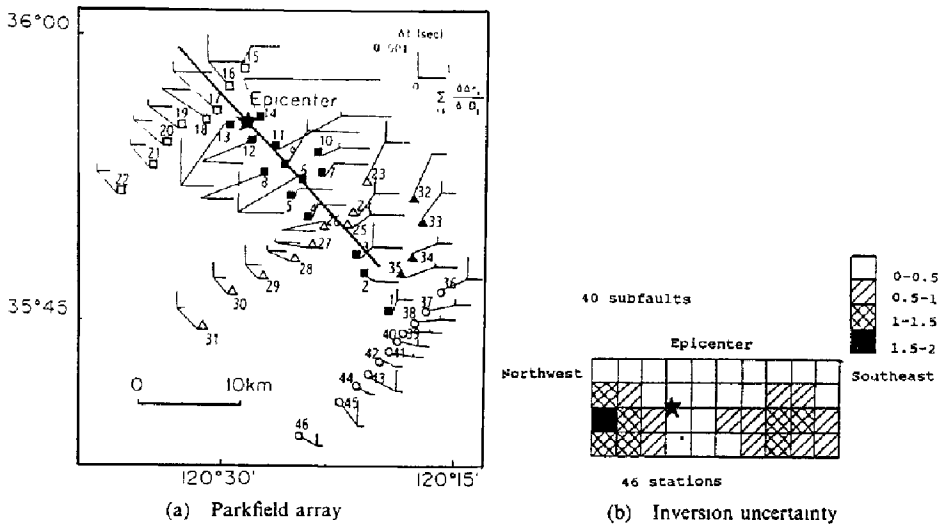

(a) Parkfield array (b) Inversion uncertainty

Fig. 4 Location map of the Parkfield section of the San Andreas fault showing the fault trace of the anticipated Parkfield earthquake and the strong-motion stations in (a) and the inversion uncertainty at all the subfaults in (b). Three arrays examined are 1) 14 stations aligned along the fault trace (the solid squares), 2) 8 stations aligned perpendicular to the fault trace added to the 14 stations (in total, 22 stations, the solid and open squares), and 3) all 46 stations. The inversion uncertainty at 40 subfaults determined for the case of 46 stations is indicated by ranking. The time separation and the moment sensitivity are also shown at each station for the case of 40 subfaults. See caption of Fig. 3 for detailed explanations.

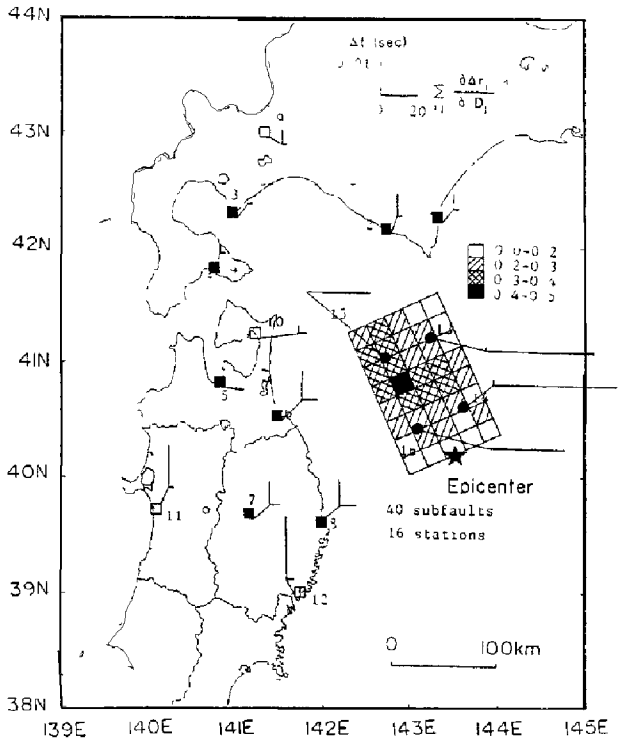

Fig. 5 Location map of the Tokachi-Oki region showing the fault area of the 1968 Tokachi-Oki earthquake and the strong-motion stations. Three arrays examined are 1) 8 land stations (the solid squares), 2) 12 land stations including one hypothetical station numbered 10 in the figure (the solid and open squares), and 3) 4 hypothetical ocean bottom stations (the solid circles) added to the 12 land stations (in total, 16 stations). The inversion uncertainty at 40 subfaults determined for the case of 16 stations is indicated by ranking. The time separation and the moment sensitivity are also evaluated at each station for the case of 40 subfaults. See caption of Fig. 3 for detailed explanations.

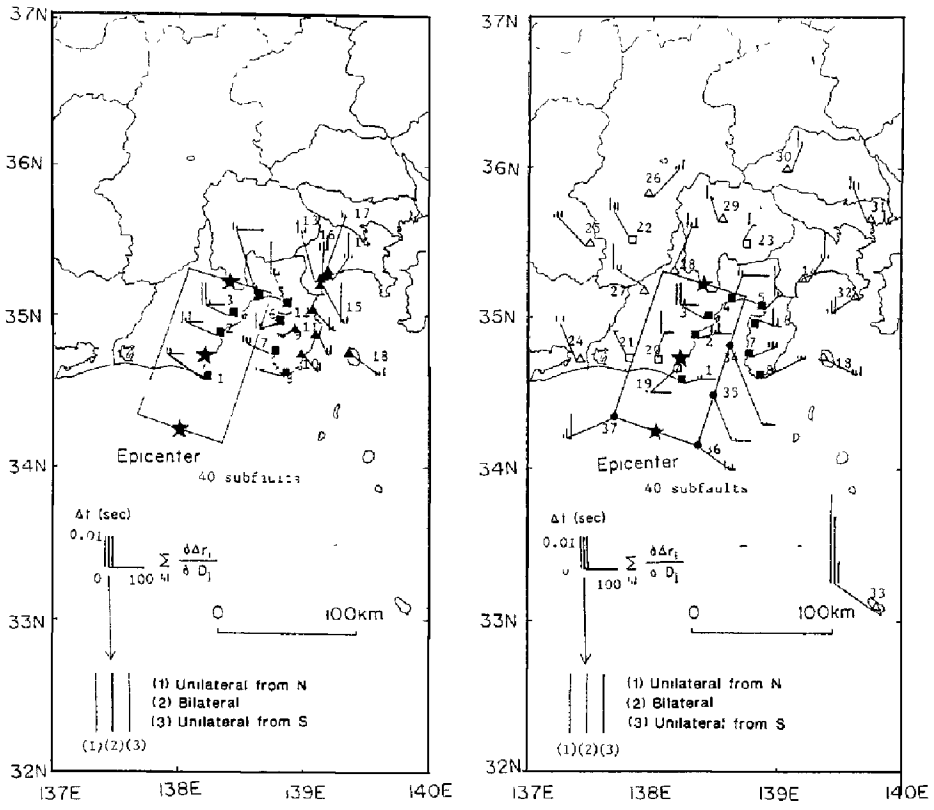

(a) Arrays with 8 and 18 stations

(b) Arrays with 13, 25 and 29 stations

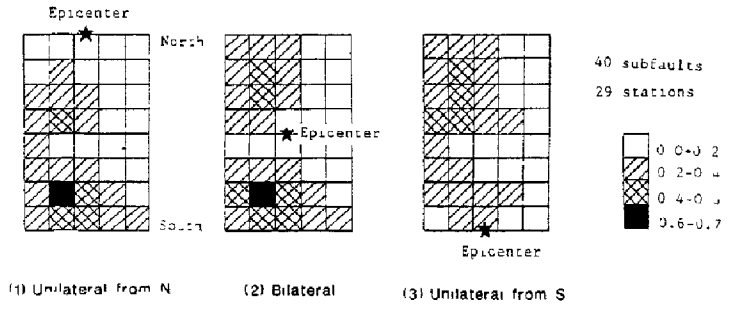

(c) Inversion uncertainty

Fig. 6 Location map of the Tokai region showing the fault area of the anticipated Tokai earthquake and the strong-motion stations in (a) and (b), and the inversion uncertainty calculated at all the subfaults in (c). Five arrays examined are 1) 8 stations of the Suruga-Izu array (the solid squares), 2) all 18 stations of the Suruga-Izu array (all the stations shown in (a)), 3) 13 land stations (the solid and open squares in (b)), 4) 25 land stations including 4 hypothetical ones numbered 25 to 28 in panel (b) (the squares and the open triangles in (b)), and 5) 4 hypothetical ocean bottom stations (the solid circles in (b)) added to the 25 land stations (29 stations in total, all the stations shown in (b)). The inversion uncertainty at 40 subfaults calculated for the case of 29 stations and for the three rupturing modes (unilateral rupture propagation starting from the northern end, bilateral from the center of the fault, and unilateral from the southern end) is illustrated by ranking. The two key parameters are also evaluated for the case of 40 subfaults. The time separation is shown for the three cases of rupturing. See caption of Fig. 3 for detailed explanations.

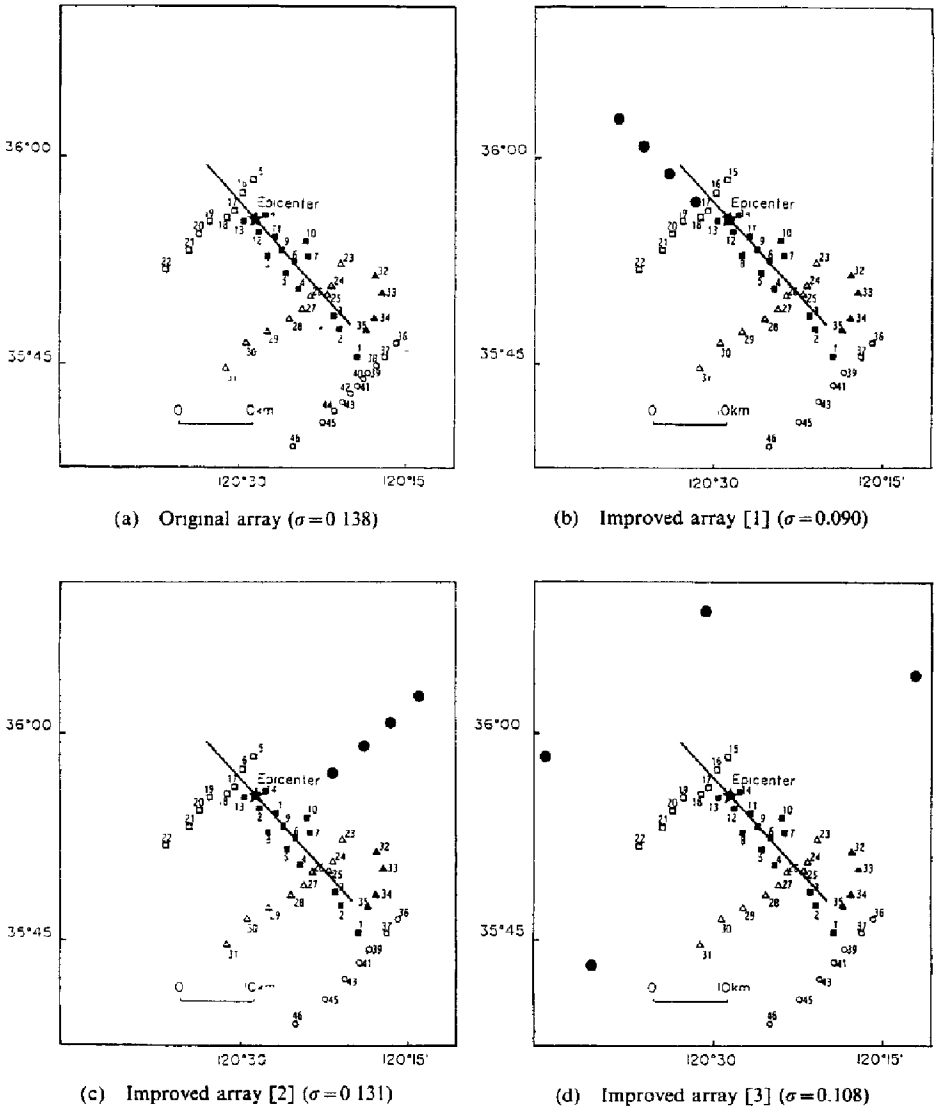

(a) Original array ($\sigma = 0.138$)

(b) Improved array [1] ($\sigma = 0.090$)

(c) Improved array [2] ($\sigma = 0.131$)

(d) Improved array [3] ($\sigma = 0.108$)

Fig. 7 Three kinds of station arrays -- (b), (c) and (d) -- tested for the improvement of the resolving power of the Parkfield array compared with the original array, (a). Tested arrays are formed by relocating four stations numbered 38, 40, 42 and 44 in the original array. The maximum normalized standard deviation of the estimated subfault seismic moment is also shown in the parenthesis. The solid circles shown in panels (b), (c) and (d) indicate the relocated four stations.

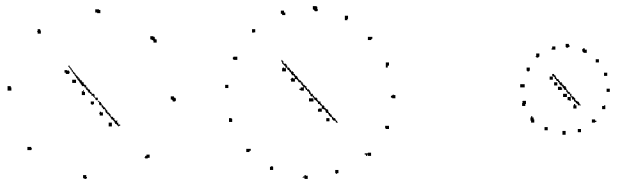

(a) 14 stations ($\sigma = 0.210$)

(b) 22 stations ($\sigma = 0.149$)

(c) 30 stations ($\sigma = 0.130$)

Fig. 8 Desirable array configurations for the Parkfield section of the San Andreas fault together with the maximum uncertainty estimated for each array. Note that the 30-station array (c) has slightly better resolving power (the maximum normalized uncertainty is 0.130) than that of the actual Parkfield array of 46 stations (0.138).